X-ray-diffraction study of the crystal structures and orientational glass state of $Ar_{1-x}(N_2)_x$ solid solutions

H. Klee and K. Knorr
Institut für Physik, Universität Mainz, 6500 Mainz, Federal Republic of Germany
(Received 21 December 1989; revised manuscript received 6 April 1990)

Solid solutions of $Ar_{1-x}(N_2)_x$ have been investigated by x-ray powder diffraction in the range $0.5 < x < 1.0$, $8 < T < 60$ K, and under hydrostatic pressures up to 2200 bars. The structural hcp-cubic ($Pa3$) phase transition is identified as a martensitic transformation with a wide transformation hysteresis. For $x < 0.8$ and $T < 30$ K the solid solutions show the orientational glass state, which is characterized by a superposition of inhomogeneous and homogeneous lattice strains. The inhomogeneous component is described by the random-field model. The homogeneous component corresponds to an orthorhombic distortion of the hcp lattice. Two products of the $Pa3$ phase have been detected: an orientationally disordered fcc state and the high-pressure γ modification. It is concluded that the $Pa3$ phase and its products have no direct relevance to the orientational glass state. The analogies to the glasslike state of the mixed cyanides and of ortho-para-H_2 are worked out.

I. INTRODUCTION

A quadrupolar orientational glass state has been observed in three series of mixed crystals: $(para\text{-}H_2)_{1-x}(ortho\text{-}H_2)_x$ (Refs. 1 and 2), mixed cyanides[3] like $(KBr)_{1-x}(KCN)_x$, and $Ar_{1-x}(N_2)_x$ (Refs. 4–12). For $x=1$, where the aspherical species (N_2, CN^-, o-H_2) is fully concentrated, a phase transition from a dynamically disordered high-temperature phase to an orientationally long-range-ordered low-temperature phase occurs. Upon dilution with a spherical component (Ar, Br^-, p-H_2) the transition temperature decreases and vanishes at a threshold concentration x_c (see, e.g., Fig. 1). For concentrations below x_c the orientations of the aspherical component freeze-in randomly at low T and the high-temperature center-of-mass lattice is preserved down to the lowest temperatures.

For Ar:N_2 (and o-p-H_2) the dynamically disordered high-T β phase is hcp.[12] At least for pure N_2 it is known[13,14] that the molecules precess around the c axis with an inclination angle which is close to the magic angle of 54.7°. This means that the time-averaged quadrupole moment of the N_2 molecule approximately vanishes. Accordingly, the c/a ratio is close to the ideal value of the hexagonal close packing of spheres.

The low-T ordered α phase of N_2 and the N_2-rich Ar:N_2 mixed crystals is cubic. The center-of-mass lattice is fcc: the N_2 orientations are arranged in a four-sublattice pattern.[15] In each of the sublattices the molecules are parallel along one of the ⟨111⟩ directions (space group $Pa3$).

For Ar:N_2 the formation of the orientational glass state is evidenced from inelastic-neutron-scattering[4] and NMR experiments.[5–7] It has been concluded that the orientational degrees of freedom freeze-in rather gradually. Specific-heat,[8,9] thermal-conductivity,[10] and dielectric experiments[11] (on Ar:CO:N_2) have confirmed the glassy character of this state of frozen-in orientations, showing a linear specific heat, an excess Debye contribution, a plateau in the thermal conductivity, and a dielectric relaxation with a broad distribution of barrier heights. A model explaining these observations by assuming the existence of two-level systems with a distribution of energy barriers and energy differences between the two minima

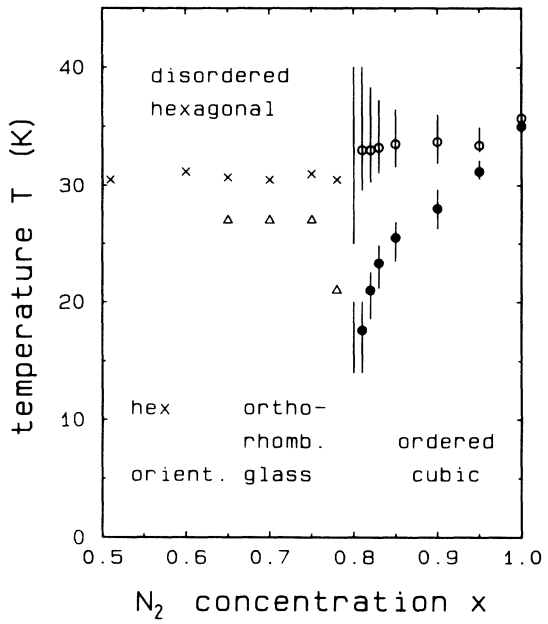

FIG. 1. x,T phase diagram of $Ar_{1-x}(N_2)_x$ under its own vapor pressure. The hcp-cubic transition temperatures are defined as temperatures where the diffraction lines of the two phases are of comparable intensity (circles). Solid symbols refer to slow cooling and open symbols to slow heating. The bars indicate the width of the hcp-cubic coexistence region (see Sec. IV B). The freezing temperatures T_f (crosses) are derived from the T dependence of the width of the powder lines (as discussed in Sec. IV E). The triangles denote the temperatures, where the orthorhombic distortion becomes detectable (see Sec. IV F).

of the postulated double-well potential has been developed for the cyanides.[16] Its application to Ar:CO:N_2 has been studied in Ref. 9.

For the cyanides, detailed theoretical investigations of the orientational glass state have been based on a random-field model,[17–20] random strain fields being introduced by the substitution of ions with slightly different sizes. On the other hand, *o-p*-H_2 is traditionally described by a random-bond model[2] known from spin glasses.[21] The application of the random-bond model to quadrupolar glasses has been studied by mean-field theory[22] and by computer simulations for hexagonal[23] and cubic lattices.[24,25]

Two different phase diagrams obtained by x-ray diffraction have been reported in the literature: samples grown from the melt show complete miscibility;[12] samples vapor-deposited on a cold surface show a large miscibility gap.[26] [Effects of the preparation technique on the crystal structure are also known for *o-p*-H_2 and -D_2 (Refs. 1 and 27).] Despite the fact that the x, T phase diagrams of *o-p*-H_2, Ar:N_2, and the mixed cyanides are analogous, the structural data illuminate essential differences, as pointed out in the following.

For the mixed cyanides the orientation-transition coupling leads to a variety of ferroelastic phases,[28,29] which can be derived from the cubic high-temperature phases by combinations of three independent shear deformations of T_{2g} symmetry and by a concomitant alignment of the CN molecules. The competition between the homogeneous shear deformation and the tendency of a macroscopic crystal to keep its shape leads to multidomain states with regular domain patterns in the pure cyanides and in the mixtures with high CN^- concentrations.[3] The orientational glass has been regarded as a short-range-ordered variety of the ferroelastic phases, with locally polarized regions being the analog of the domains of the long-range-ordered phases. The statistical variation of these local distortions corresponds to a distribution of lattice strains, observable in x-ray experiments as broadening of the diffraction lines.[30–32] It is the aim of the present study to investigate whether this concept can be transferred to Ar:N_2.

For *o-p*-H_2 and Ar:N_2 the orientationally ordered phase is not a ferroelastic variety of the disordered high-temperature phase. There is even not a group-subgroup relation between the disordered and the ordered phase; instead the formation of the ordered phase is accompanied by a rearrangement of the center-of-mass lattice, which can be visualized by a change of the stacking sequence. Thus the question arises whether the ordered phase ($Pa3$) is of any relevance to the glasslike state, as the similarity of the Ar:N_2 phase diagram to that of the mixed cyanides might suggest.

Orientationally ordered variants of the hexagonal lattice, which might be the analog of the ferroelastic phases of the cyanides, have been predicted theoretically,[33–37] but never found experimentally for Ar:N_2 or *o-p*-H_2. For Ar:N_2, detailed structural data on the orientational glass regime do not exist. Therefore an x-ray investigation has been undertaken in this work. Application of hydrostatic pressure clarifies the relationships of the observed phases with respect to each other.

The remainder of this paper is organized as follows: In Sec. II we describe the details of the two experimental setups, for low and high pressure. In Sec. III we present the experimental results and data-reduction procedures. In Sec. IV the results are discussed, concerning (A) the phase diagram, (B) the α-β transition, (C) the ordered low-T α phase, (D) stacking faults, (E) the orientational glass, (F) the ferroelastic instability, and (G) the application of high pressure. In Sec. V we summarize the results and draw conclusions.

II. EXPERIMENT

A closed-cycle refrigerator was used to reach temperatures down to 8 K. The temperature was controlled to better than ± 0.1 K. Cu $K\alpha$ x rays emerging from a conventional tube operating at 1.2 KW were reflected from a graphite monochromator ($\lambda = 1.5418$ Å). The diffractometer was set up in Bragg-Brentano geometry. The position-sensitive detector covered an arc of $\pm 6°$ around its mean 2θ position. The instrumental resolution was 0.25° full width at half maximum (FWHM) at $2\theta \cong 40°$, as derived from the linewidth of BN ($hk0$) and of Ar:N_2 high-temperature (hcp) reflections.

Gases of high purity (> 99.9997%) were mixed at room temperature and condensed into the probe chamber at 65 K. The liquid was allowed to homogenize for 1 h. Since the amount of gaseous Ar:N_2 in the filling capillary (0.1 cm^3 STP) was small compared to the liquid Ar:N_2 in the probe chamber (typically 100 cm^3 STP), the change in concentration due to the different vapor pressures of Ar and N_2 was negligible.

The cell was stuffed with BN powder, which serves two purposes: (i) BN reflections are an internal standard for the determination of the lattice parameters of Ar:N_2; (ii) condensing Ar:N_2 into the pores of the BN matrix considerably improved the quality of the samples in the sense of powder diffractometry by reducing the effects of preferred orientations. However, we could not suppress these effects completely and hence will not evaluate Bragg intensities in a quantitative way. It was verified that this procedure does not affect the position and width of the Ar:N_2 reflections. The plane sample surface, needed for the reflection of x rays in parafocusing geometry, was provided by a Kapton foil of thickness 0.02 mm (Fig. 2).

The powder quality of the samples was further improved by solidifying the liquid by rapid cooling (cooling rate 5 K/min) from a temperature slightly above the melting temperature down to 50 K. The sample was annealed at 50 K for 1 h in order to remove internal strains. Subsequently, the sample was cooled down in steps of typically 5 K. At each step x-ray profiles were taken at four positions of the position-sensitive detector, such that an angular range $20° < 2\theta < 60°$ was covered. Seven to ten Ar:N_2 Bragg reflections were observable in this range. It was necessary to reduce the cooling rate during the 5-K steps to 0.5 K/min; otherwise a shift in the hcp-cubic transition temperature, a suppression of the orthorhombic distortion (see Sec. IV F), and an increase of the inho-

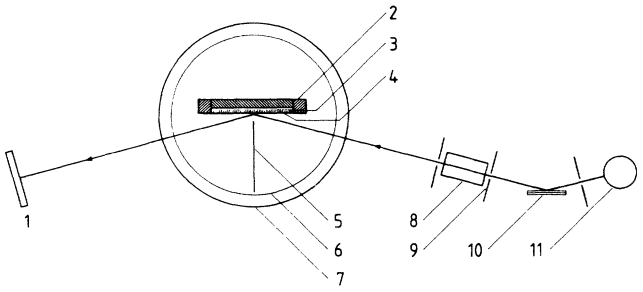

FIG. 2. Experimental setup for investigations of Ar:N_2 under its own vapor pressure: 1, position-sensitive detector; 2, copper frame; 3, probe chamber containing BN powder and Ar:N_2; 4, Kapton foil; 5, x-ray shield; 6, thermal shield; 7, vacuum jacket with Be window; 8, Soller slits; 9, vertical slits; 10, monochromator; 11, x-ray tube.

mogeneous strains was observed. It was verified that a reduction of the cooling rate by a factor of 10 did not change the results any further. After the minimum temperature of 8 K was reached, subsequent stepwise heating to 60 K completed the measuring cycle.

In a second set of experiments, hydrostatic pressure was applied. He gas was pressurized up to 2200 bars by an air-driven diaphragm compressor. Gas-leading parts and the probe chamber had to be changed to withstand these pressures. A thick-walled Be capillary was used as a probe chamber (Fig. 3). Strong Be- and weak Be-oxide reflections contaminated the spectrum and prevented the observation of more than the first three Ar:N_2 reflections. The capillary was not filled with BN in order to avoid the

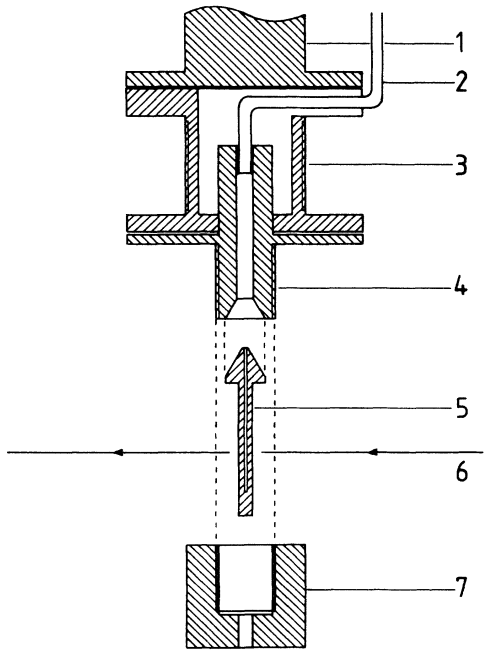

FIG. 3. High-pressure cell: 1, cold head; 2, thick-walled steel filling capillary; 3, heater; 4, socket with conical seat for Be probe chamber; 5, thick-walled Be capillary containing Ar:N_2; 6, x-ray beam; 7, nut.

screening of one of these few Ar:N_2 reflections by a BN reflection. Thus a different technique of producing powders acceptable for x-ray powder diffraction was applied: The liquid was condensed into the Be cell at low pressure and then solidified within fractions of a second by applying pressure. Subsequently, the sample was cooled to 50 K as quickly as possible to avoid the coalescence of the crystallites. It was important not to overfill the sample cell; otherwise the pressure in the sample was not necessarily identical to the pressure read by the pressure gauge. The actual pressure of the sample could be estimated by referring to the literature values on the pressure dependence of the hcp-cubic transition temperature and of the lattice parameters of pure N_2 (Refs. 38 and 39).

III. RESULTS

Fifteen concentrations have been studied at low and at high pressures. The counting time for the x-ray spectra was 20 min. For the low-pressure experiments, the maximum height of the Bragg peaks was about 3000 counts for the weakest and 100 000 counts for the strongest peaks, above a background of 3000 counts. For the high-pressure setup, the Bragg peaks were about a factor of 10 smaller due to the absorption of the thick-walled probe chamber. The background was about 2000 counts (for an example, see Figs. 13 and 14). Strong Be reflections (150 000 counts) and weak BeO reflections (3000 counts) masked the Ar:N_2 reflections at $2\theta \gtrsim 35°$.

Gaussian profiles were fitted to the observed spectra. The lattice parameters were determined by a least-squares fit to the positions of ten Bragg reflections and were converted to molar volume [Figs. 4, 7, and 8(a)] and c/a ratio (Fig. 5). The observed linewidth (Fig. 10) was converted to the intrinsic width, assuming that the instrumental resolution adds quadratically to the intrinsic width. This is a good approximation since the observed line shapes are close to Gaussian.

The x, T phase diagram is shown for low pressure in Fig. 1 and for high pressure in Fig. 8(b). The hexagonal-cubic transition temperatures have been determined from plots of the line intensities versus T (Fig. 6).

IV. DISCUSSION

A. Phase diagram

The x, T phase diagram as derived from the present study is shown in Fig. 1. As far as the miscibility of the two species and the approximate size of the $Pa3$ field is concerned, it is in general agreement with that of Barrett and Meyer.[12] The lowest N_2 concentration of the present study falls into the range where these authors observed a fcc low-T state after cold working. We never observed this phase, though we used several types of annealing cycles and applied hydrostatic pressure.

Figure 4 displays the molar volume of the hcp phase at 50 K as a function of x. It shows a positive departure from Vegard's law [as obtained by an interpolation between N_2 (Ref. 13) and Ar (Ref. 40)], but otherwise varies smoothly with x, a fact which suggests that chemical

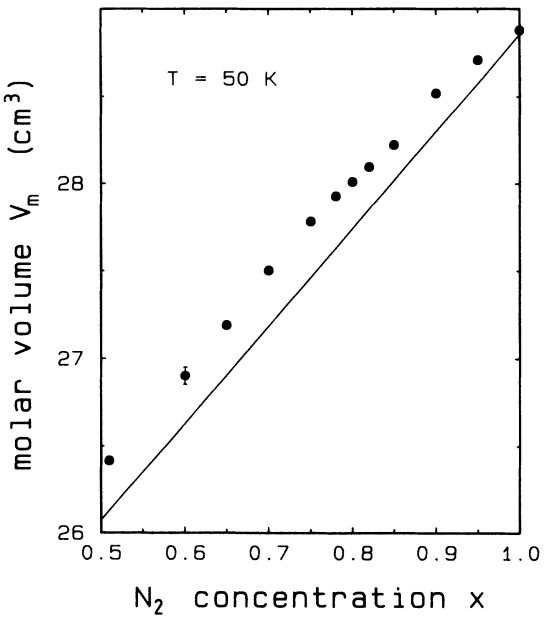

FIG. 4. Molar volume of Ar:N_2 under its own vapor pressure vs N_2 concentration x. The solid line connects the literature values for pure N_2 and pure Ar.

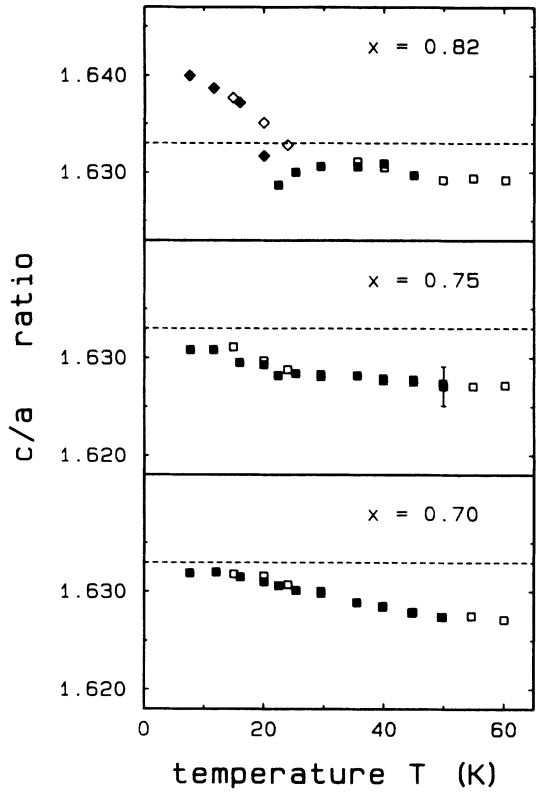

FIG. 5. Hexagonal c/a ratio for three different concentrations. For $x=0.82$ the diamonds indicate the c/a ratio of the 10% residual hcp amount in the $Pa3$ phase. Open symbols refer to cooling and solid symbols to heating. Dashed horizontal lines give the ideal value for the close packing of spheres of $\sqrt{8/3}=1.633$.

decomposition does not occur.

For all x,T values the c/a ratio of the hcp phase is close (within 0.5%) to the ideal value. Nevertheless, significant departures exist: For $x \leq 0.95$, c/a is slightly below ideal in the whole T range investigated; c/a increases with decreasing T (Fig. 5).

B. α-β transition

The hexagonal and cubic structures are easily distinguished by inspection of the strong hcp (101) and cubic (200) reflections, which are well separated in 2θ from reflections of the other phase. In Fig. 6 the intensities of these two reflections are plotted versus temperature for two concentrations. The temperatures where the intensities pass 50% of their saturated values are regarded as transition temperatures T_{hc} and T_{ch}, respectively (circles in Fig. 1). The characteristic temperatures M_s, M_f, A_s, and A_f of the martensitic hysteresis loop[41] are indicated in Fig. 6. The widths of the hcp-cubic coexistence regions, given by M_s-M_f and A_f-A_s, are indicated as bars in Fig. 1. For pure N_2 the transformation is sharp. The small thermal hysteresis is $\Delta T = T_{ch} - T_{hc} = 0.7$ K, a value which agrees with Ref. 15. With increasing Ar content the transformation loop is progressively broadened to about $\Delta T = 15$ K for $x=0.81$ (also see Fig. 1). When samples were kept for periods up to 14 h at constant temperatures within the coexistence regions, there was no change of the peak intensities with time. Such a behavior is characteristic of an athermal martensitic transformation.[41] (The same conclusions[1] have been drawn in o-p-H_2 too.) Surprisingly, Barrett and Meyer[12] did not mention coexistence regions and hysteresis effects in their diffraction study on Ar:N_2.

Upon heating, cubic reflections always remain visible up to 40–45 K. However, in contrast to o-p-D_2, this cubic residue could not be increased by repeated thermal cycling through the transition. Furthermore, there are no indications that parts of the sample transform into parasitic structures, which are neither cubic nor hexagonal, unlike to o-p-D_2 (Ref. 42). The hcp-to-cubic transformation of samples with x around $x_c = 0.8$ is incomplete, the cubic fraction at low temperatures varying from 90% at $x=0.82$ to 10% at $x=0.79$. For $x<0.75$ cubic residues do not occur any more.

In Fig. 7 the molar volume is plotted versus temperature for three different concentrations. For $x > x_c$ the volume jump ΔV_m at the hcp-to-cubic transition has been determined and is plotted versus x in Fig. 8(a). ΔV_m changes sign at $x=0.85$: For $x>0.85$ the low-temperature phase has the smaller volume, and for $x<0.85$, the larger volume. (A corresponding change of sign in the pressure jump at the transition, Δp at constant volume, has been reported in the literature[43] for o-p-H_2.) The molar heat of transformation Λ is related to the slope dp/dT of the phase transition line in the p,T phase diagram in terms of the Clausius-Clapeyron equation:

$$\Lambda = \Delta V_m T_{hc} \frac{dp}{dT} . \quad (1)$$

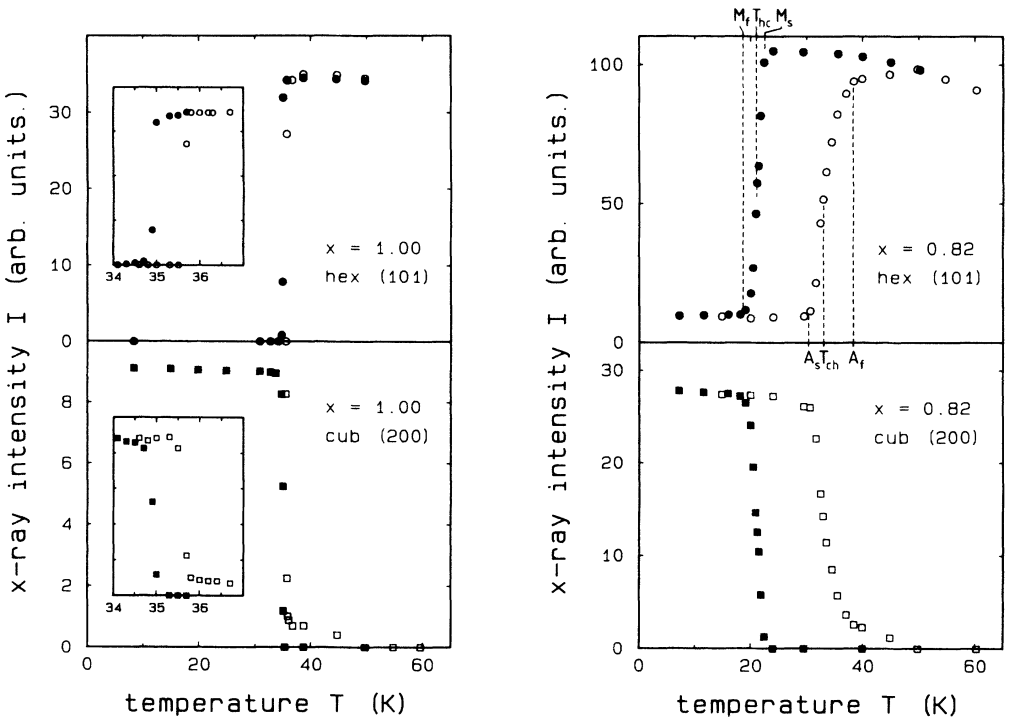

FIG. 6. Intensities of x-ray powder reflections $(101)_{hex}$ and $(200)_{cub}$. These reflections are "pure," i.e., not contaminated by reflections of the other phase. For $x=1.0$, the inset shows the sharp transition in detail. Open symbols refer to cooling and solid symbols to heating.

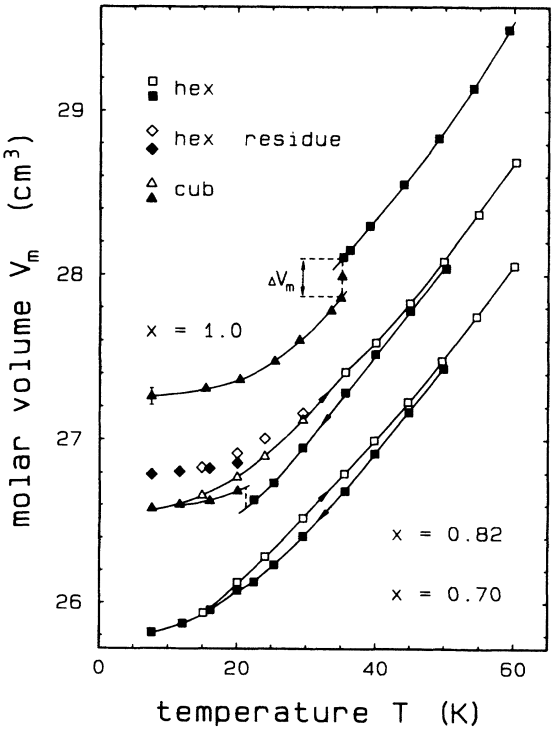

FIG. 7. Molar volume for three different concentrations. For $x=1.0$ and 0.82 we indicated how the volume jump ΔV_m at the hcp-to-cubic transition was determined. Open symbols refer to cooling and solid symbols to heating. The solid lines are guides to the eye.

Thus dp/dT has to change sign when ΔV_m changes sign. As seen in Fig. 8(b), the transition temperatures T_{hc} and T_{ch} are indeed shifted to higher values for $x>0.85$, whereas for $x<0.85$ T_{hc} is shifted to lower values and T_{ch} remains constant when pressure is applied.

The threshold concentration for ordering, x_c, is changed to a value slightly larger than 0.82. These results are obtained if samples are cooled under pressure. Cooling first and pressurizing afterwards gives different results (see Sec. IV G). Using Eq. (1), Λ has been determined from cooling results and compared to calorimetric results of Refs. 8 and 44 in Table I. The values of Λ as determined by the two methods agree within the experimental error. Λ is reduced when approaching x_c, but remains finite. In principle, the results obtained upon heating rather than those obtained upon cooling should be compared to specific-heat data, but (i) the cubic-to-hcp transition upon heating does not correspond to the specific-heat peak as discussed in Sec. IV C, (ii) ΔV_m upon heating is undetectably small for $x<0.9$, and (iii) T_{ch} is insensitive to pressure. These points render the application of Eq. (1) to the heating data impossible.

C. Ordered low-T α phase

The orientational order of the $Pa3$ structure gives rise to a finite intensity of the mixed reflections (hkl) with h,k,l partially odd and partially even, such as (210), (211), (221), and (320), in addition to the other fcc-type reflections. For pure N_2 these mixed, $Pa3$-specific

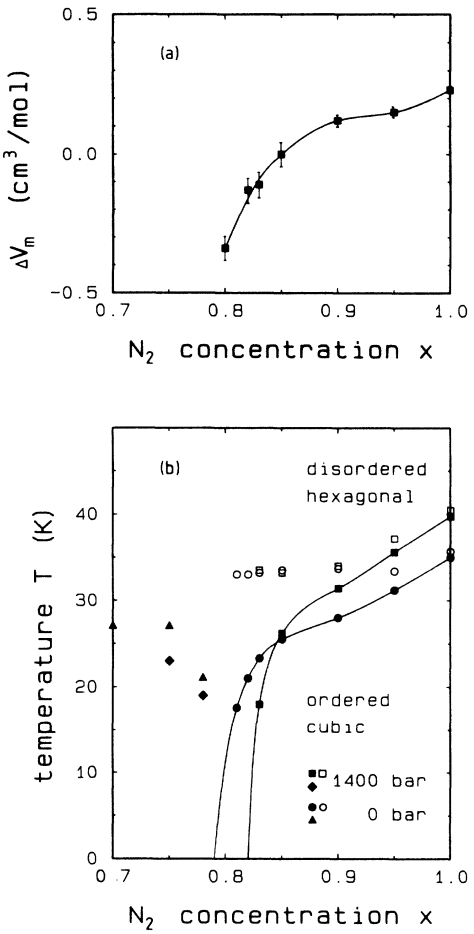

FIG. 8. (a) Jump in the molar volume at the hcp-to-cubic transition, changing sign at $x=0.85$. (b) Phase diagram with transition temperatures: open circles, T_{ch}(0 bar); solid circles, T_{hc}(0 bar); open squares, T_{ch}(1400 bars); solid squares, T_{hc}(1400 bars). For clarity, the hexagonal-cubic coexistence regions have been omitted in this figure; the widths of these regions are practically unchanged by application of pressure. The temperatures where the orthorhombic distortion becomes detectable are indicated by triangles ($p=0$ bar) and diamonds ($p=1400$ bars). The solid lines are guides to the eye.

reflections are observed throughout the whole temperature regime of the cubic phase. We emphasize this point because the loss of orientational order in the cubic state in the temperature interval $(T_{ch}-10\ \text{K}) < T < T_{ch}$ has been suspected from recent Raman experiments[45] on pure N_2. Cooling down mixtures with $x \leq 0.95$, the $Pa3$-specific reflections again occur exactly at the hexagonal-to-cubic transition temperature T_{hc}. However, starting from the $Pa3$ phase, upon heating, the $Pa3$-specific reflections vanish at a characteristic temperature T_{or}, well below the cubic-to-hexagonal transition temperature T_{ch}. Thus an orientationally disordered fcc-like state is suggested for $T_{or} < T < T_{ch}$. The following transition scheme is obtained:

$$\text{cooling: disordered hcp} \xrightarrow{T_{hc}} \text{ordered cubic ,}$$

$$\text{heating: ordered cubic} \xrightarrow{T_{or}} \text{disordered cubic} \xrightarrow{T_{ch}} \text{disordered hcp .}$$

T_{or} is larger than T_{hc}. Note that T_{ch} can exceed T_{hc} by as much as 15 K. Unfortunately, the diffraction profiles have been recorded with relatively coarse T steps in the vicinity of T_{or}, so that an exact determination of T_{or} will need future experimental work. Within the accuracy so far available, T_{or} coincides with the temperatures where specific-heat anomalies have been observed,[8,44] e.g., $T_{or}=27\pm2.5$ K for $x=0.83$, compared to the value of the specific-heat work,[44] $T_{\text{trans}}=25.6$ K. Obviously, the specific-heat anomaly is due to the transition from orientational order to disorder and not to the reconstruction of the center-of-mass lattice. At the cubic-to-hexagonal transition temperatures determined by the present work, specific-heat anomalies have not been reported in Refs. 8 and 44. This point suggests that the energy difference between the hcp and fcc structures is small.[46] Very analogous phenomena have been found in o-p-D_2 (Refs. 1 and 43), where thermal cycling was needed to stabilize the disordered fcc state. For Ar:N_2 one arrives at the same picture that has already been formulated for o-p-D_2 (Ref. 1): At high T, the disordered hcp is the stable structure. Slightly above T_{or}, disordered fcc is more stable than hcp. However, starting from hcp, the potential barrier for the reconstruction of the center-of-mass lattice prevents the appearance of fcc structure. Below T_{hc} the quadrupole-quadrupole interaction drives the hcp-to-fcc transition, because the lowest energy can be achieved when ordered on fcc. Starting from the $Pa3$ phase, upon heating, the most stable structure slightly above T_{or}, disordered fcc, is

TABLE I. The hcp-to-cubic transition temperatures $T_0=T_{hc}(p=0$ bar), $T_p=T_{hc}(p=1400$ bars); the jump in the molar volume, ΔV_m, at the hcp-to-cubic transition; the molar heats of transformation Λ_x, calculated from x-ray results (see text); and Λ_c, obtained from specific-heat experiments (Refs. 8 and 44).

x	T_0 (K)	T_p (K)	ΔV_m (cm^3/mol)	Λ_x (cal/mol)	Λ_c (cal/mol)
1.00	35.0±0.1	39.8±0.5	0.22±0.02	54±5	54.68
0.95	31.2±0.2	35.6±0.5	0.15±0.02	46±7	
0.94					45.64
0.90	28.0±0.2	31.4±0.5	0.12±0.02	33±6	37.16
0.85	25.5±0.5	26.2±0.5	0.00±0.05		
0.83	23.3±0.5	18.0±0.5	−0.11±0.05	17±8	21.18

favored. Thus the $Pa3$ phase has to be entered first; otherwise the disordered fcc phase does not occur, but thermal cycling is not needed, unlike the case of o-p-D_2.

D. Stacking faults

The two center-of-mass lattices observed in Ar:N_2, fcc and hcp, can be regarded as different stacking sequences of close-packed $(111)_{cub}/(001)_{hex}$ planes, following the schemes $ABCABC\ldots$ and $ABAB\ldots$, respectively. Thus stacking faults are of importance for the hcp-cubic transformation and perhaps even for the formation of the orientational glass state. One distinguishes deformation faults, caused by a translation of the whole crystal parallel to the basal planes above the fault plane, and growth faults, caused by a change of the stacking rule during the growth process. Faults lead to a broadening and to shifts of the powder lines.[47–49]

Following the explicit expressions of Ref. 48 for fcc and hcp lattices, we extracted the growth-fault probability α and the deformation-fault probability β from the width and shift of the lines. The systematics of these effects as a function of the line index allowed us to discriminate against other sources of line broadening, such as finite-size effects.

The results for the stacking-fault probabilities are shown in Fig. 9 for $x=0.82$. The results on samples with other concentrations are analogous. In the hexagonal phase, $\alpha=0$ within the accuracy of the experiment. Deformation faults (β_{hex}) are presumably produced by mechanical stresses which arise as a consequence of the large thermal contraction of Ar:N_2. In the hcp-fcc coexistence region, β_{hex} is slightly enhanced. In the cubic phase the growth fault dominates. For the fcc lattice the growth fault is a twin fault. Twinning at the hcp-to-fcc transformation can be explained as follows: According to the periodic-slip mechanism,[49] the martensitic hcp-fcc transformation can be visualized as periodic slip of basal planes parallel to one out of six possible slip vectors lying in the planes. An eventual change of the slip direction produces twin faults.

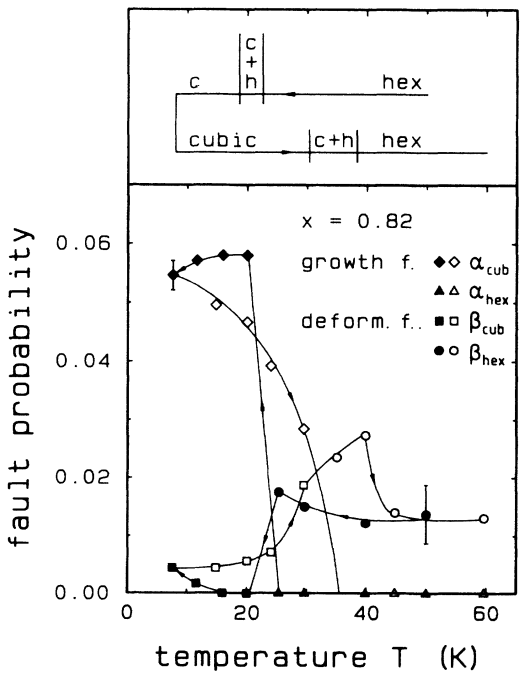

FIG. 9. Stacking faults: deformation-fault probabilities β and growth-fault probabilities α vs T for $x=0.82$. Open symbols refer to cooling and solid symbols to heating. The solid lines are guides to the eye. The top of the figure visualizes the path through the phases.

In the concentration regime $0.5<x<x_c$, hexagonal deformation faults can be detected at high temperatures ($T>40$ K), analogous to the results for $x>x_c$. With decreasing temperature a strong additional type of line broadening is observed, which concerns all reflections and increases with wave vector Q. For the hcp reflection (110), which is not affected by stacking faults, the line broadening is especially strong. Therefore the possibility that stacking faults are the source of the line broadening in the orientational glass regime can be excluded.

E. Orientational glass

As the orientational glass evolves out of the high-T phase, the molar volume decreases smoothly with T (Fig. 7). The slight deviation between cooling and heating for $12<T<30$ K is observed for all concentrations $0.65\le x\le 0.78$. This is the first time that hysteresis effects are seen in an orientational glass. The origin of this hysteresis is unknown. The c/a ratio is displayed in Fig. 5. For $x<x_c$ no phase-transition-like onset of the orientational glass state is seen. The anomaly for $x=0.82$ is connected with the hcp-cubic phase transition. Here at low T the c/a ratio of the 10% residual hcp amount is plotted.

The most striking feature of the orientational glass is the strong broadening of the Bragg lines with decreasing temperature (see Fig. 10), which is reminiscent of the line broadening in the glass-forming cyanides.[29] In the cyanide single crystals the linewidth increased about linearly with the line index. Such a behavior suggests that the broadening is due to a distribution of lattice parameters[47] (as observed, e.g., in cold-worked metals) and not to a fragmentation of the crystal or statistical variations of the next-neighbor distance (paracrystalline model[50,51]). In the present powder results the experimental information is sufficient for a clear-cut distinction between these different broadening mechanisms, and additionally the stacking faults. Nevertheless, there is clear indication that the formation of the glass state leads to a dominant type of line broadening which involves all lines and which scales about linearly with $|\mathbf{Q}|$. Thus we suggest that inhomogeneous lattice strains develop in the orientational glass, and we conclude that the orientations are coupled to the lattice strains. For the mixed cyanides this coupling leads to an instability with respect to shear deformations and thus to the ferroelastic phases for $x>x_c$. For $x<x_c$, Bragg lines which would show the strongest splitting in the ferroelastic phases show the strongest broadening in the orientational glass.[29] For

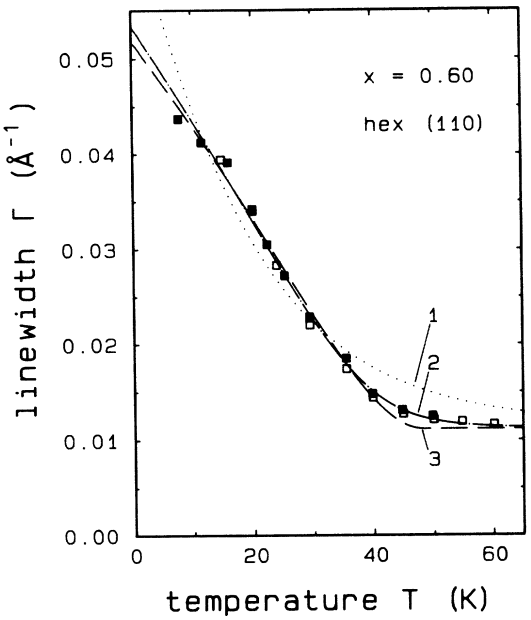

FIG. 10. Apparent linewidth (FWHM) of the hcp (110) reflection for $x=0.60$. Dashed lines show the result of three least-squares fits: 1, pure random fields, $J=0$; 2, $\Delta/J^2=0.05$; 3, pure random bonds, $\Delta=0$. For details, see text. Open symbols refer to cooling and solid symbols to heating

Ar:N_2 the broadening is strongest for $(hk0)$ reflections, suggesting an instability with respect to a shear of the cell angle γ. For $0.65 \lesssim x \leq x_c$ even a homogeneous ferroelastic strain component is observed (see Sec. IV F), which develops in addition to the inhomogeneous strains.

The inhomogeneous component of the strains is a basic feature of the random-field model developed by Michel[18] for the orientational glass state of the mixed cyanides. According to this model, disorder scattering occurs in the vicinity of the Bragg lines, the diffuse intensity or, equivalently, the width of the powder lines being proportional to the "glass order parameter" q, which is defined in a way analogous to the Edwards-Anderson glass order parameter for spin glasses.[52] For spin glasses a transition from a high-T state with $q=0$ to a low-T glassy state with $q\neq 0$ is obtained, whereas in the random-field model for orientational glasses q has nonzero values at any finite T and increases gradually as T is decreased. Within the high-temperature limit, $q=\Delta/T^2$, where Δ is the variance of the random-strain-field distribution.[18] Since predictions for $q(T)$ at low T do not exist, we apply a theoretical result obtained for a random-bond classical Ising system in a random field.[53] It is by no means clear whether this model describes quadrupolar glasses correctly, but it reproduces the high-temperature limit of Michel's model, and has been successful in fitting NMR results on the orientational glass order parameter of NaCl:NaCN (Ref. 54) and of $Rb_{0.56}(ND_4)_{0.44}D_2PO_4$ (Ref. 55).

As shown by replica mean-field theory, $q(T)$ is determined self-consistently within the Ising model by the following equation:[53]

$$q=\frac{1}{\sqrt{2\pi}}\int_{-\infty}^{\infty} dx\, \exp(-x^2/2)\tanh^2\left[\frac{(J^2q+\Delta)^{1/2}}{k_BT}x\right]. \tag{2}$$

The random bonds and the random fields are distributed independently according to Gaussian probability densities of variance J^2 and Δ, respectively. Fits with $J=0$, which would mean that quadrupole-quadrupole interactions are absent and that the N_2 molecules freeze-in independently in the presence of random fields, are not satisfactory (Fig. 10). For the pure random-bond case (i.e., $\Delta=0$) a sharp onset of $q(T)$ below a characteristic temperature T_0 is predicted followed by a linear increase $q(T)\propto T_0-T$ just below T_0. For intermediate cases the onset of $q(T)$ at T_0 is smeared out. Note, however, that the folding with the instrumental resolution leads to a rounding of the T dependence of the apparent linewidth Γ too. Thus the values of Δ/J^2 obtained from the fit are not very precise; they range between 0.03 and 0.07. Nevertheless, they suggest the dominance of random bonds over random fields, analogous to the results on NaCl:NaCN, where $\Delta/J^2=0.03$. T_0 is in the range 40–46 K. A systematic concentration dependence of T_0 or Δ/J^2 is not detected. It should be mentioned that an Almeida-Thouless-type instability line $T_I(\Delta)$ exists in the Ising model.[53] For $T<T_I(\Delta)$, Eq. (2) does not correspond to a stable solution. For $\Delta/J^2\cong 0.05$, $T_I(\Delta)\cong 0.7T_0$ (Ref. 53). Our conclusions concerning T_0 and Δ/J^2 are mainly based on $\Gamma(T)$ for T around T_0, and thereby on a temperature region where Eq. (2) corresponds to a stable solution.

Owing to the random-field contribution, a phase-transition-like onset of the orientational glass state does not exist; the order parameter q, or correspondingly the linewidth Γ, develops rather gradually with T. In this case, at the "nominal freezing temperature" T_0 an experimentally observable anomaly does not exist. Furthermore, the values obtained for T_0, $40\lesssim T_0\lesssim 46$ K, are surprisingly high compared to the "freezing temperatures" T_f reported for inelastic-neutron-scattering[4] and NMR experiments[5] ($T_f\lesssim 20$ K). Therefore we use an alternative definition of T_f: T_f is the temperature where $q(T)=\frac{1}{3}$. This definition has been used in the mixed cyanides. At this T_f the orientational susceptibility χ is maximum, both for Michel's and for the Ising model for $\Delta/J^2\cong 0.05$. [In a previous publication,[25] we defined T_f by $q(T_f)=\frac{1}{2}$, which corresponds to the position of the maximum in χ for $\Delta/J^2\cong 0.2$, and leads to 20% lower freezing temperatures than $q=\frac{1}{3}$.] In any case, T_f seems to be concentration independent and is somewhat higher than the freezing temperature reported for inelastic-neutron-scattering[4] and NMR experiments[5] ($T_f\lesssim 20$ K). This deviation may be due to the uncertainty in the definition of T_f, but also due to the fact that x-ray-diffraction, inelastic-neutron-scattering, and NMR measurements have different length scale and frequency windows and couple to the orientational degrees of freedom in different ways.

F. Ferroelastic instability

In the orientational glass regime, for $0.65 \lesssim x \leq x_c = 0.8$ and at low T, in addition to the inhomogeneous lattice strains, a homogeneous strain component is observed, causing, at least in principle, a splitting of all hexagonal reflections except $(00l)$. In the experiment, clear double-peak profiles have been observed for the hcp (110) line; in all other cases the profiles acquire an asymmetric shape only (Fig. 11). Data on hcp (110) have already been presented in a previous publication.[25] Double-peak profiles consisting of two Gaussians have been fitted to the experimental profiles of (110) and (100). The smaller of the two Gaussian components appears on the right-hand side for (100) and on the left-hand side for (110). The diffraction pattern is consistent with a slight decrease of the cell angle γ, from 120° to 119.3° at $T=8$ K and $0.65 \leq x \leq 0.8$. This result suggests that the hexagonal lattice is deformed into an orthorhombic one. The relation of the orthorhombic to the hexagonal lattice cell is shown in Fig. 12, together with the variation of γ with temperature. At higher T the orthorhombic distortion $\Delta\gamma$ falls below the detection limit. At lower T the splitting is blurred by the broadening of the individual peaks due to the inhomogeneous lattice strains. Thus it cannot be decided whether the homogeneous strain component evolves in a phase-transition-like manner at a certain temperature, or whether the small distortions of the hexagonal lattice are already present at high temperatures and increase gradually as the temperature is lowered, in analogy to the inhomogeneous strain component. Contrary to the hcp-cubic transition, no hysteresis is seen either in the splitting or in the broadening.

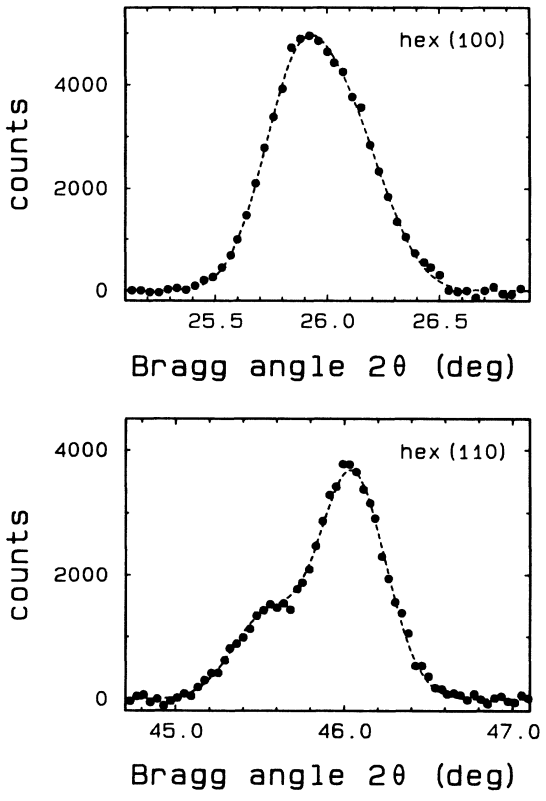

FIG. 11. Peak profiles of hcp (100) and (110) reflections. The dashed lines are the result of a least-squares fit to two Gaussians, showing the asymmetry of (100) and the splitting of (110) due to the orthorhombic distortion. A linear background has been subtracted.

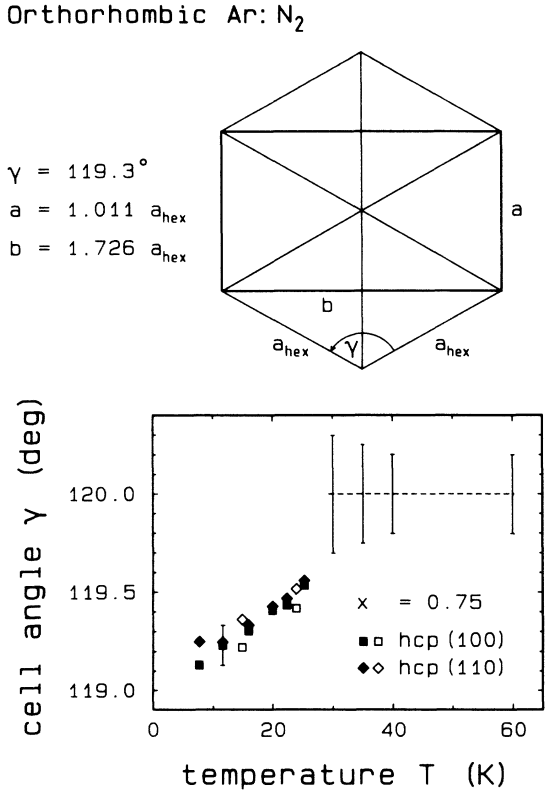

FIG. 12. Upper frame: the relation of the orthorhombic to the hexagonal lattice cell. Lower frame: cell angle γ vs temperature. The dashed line indicates $\gamma = 120°$ for the hexagonal phase; the bars denote the limits for the detection of orthorhombic distortions. Open symbols refer to cooling and solid symbols to heating.

For $0.5 < x < x_c$ the c/a ratio of the hcp phase is slightly below the ideal value, suggesting that the quadrupole moment along c is slightly negative, corresponding to an oblate orientational distribution function. The hcp symmetry requires that the moment within the basal planes vanishes. Upon freezing into the orientational glass, the ideal value is approached, if not reached. The orthorhombic distortion suggests that an in-plane quadrupole moment develops. Such an effect has been predicted by Harris and Meyer (see below).

Theoretical investigations have searched for the orientational ground state of quadrupoles on a rigid hexagonal center-of-mass lattice.[33–37] Several ordered structures with comparable binding energies have been found. Some of these ordered arrays correspond to orthorhombic superstructures, and it seems likely that the center-of-mass lattice would relax into an orthorhombic distorted variant of the hcp lattice. All these structures suggested theoretically are characterized by additional superlattice reflections, which, however, have not been observed

in the present study. In the neutron diffraction study[4] on a single crystal of $Ar_{0.28}(N_2)_{0.72}$ at 10 K, some broad maxima have been observed in the diffuse elastic intensity. In a powder-diffraction study such weak diffuse intensity is beyond the detection limit. The maxima have been attributed to frozen-in short-range orientational correlations. The corresponding "unit cell" of these correlations has dimensions $4a$, $4b$, and $3c$. Since the structural pattern of the orientational correlations is unknown, it is not clear whether these observations are related to the orthorhombic distortion of the center-of-mass lattice observed in the present study. However, the slight orthorhombic distortion is accompanied by correlations between the N_2 orientations leading to a finite in-plane quadrupolarization, as discussed above. This point emphasizes the importance of including a coupling between the orientations and the lattice strains, as has been done for a molecular-dynamics simulation of KCl:KCN, where a noncubic orientational glass has been found.[56] This noncubic glass seems to be analogous to the nonhexagonal glass of $Ar:N_2$. Experimental indications of a noncubic glass in the cyanides have been observed for NaCl:NaCN (Ref. 28). For KCl:KCN, related phenomena have been observed after thermal cycling.[57]

In the mixed cyanides the orientational glass is regarded as a short-range-ordered variety of the long-range-ordered ferroelastic phases. Correspondingly, the combination of homogeneous and inhomogeneous strains observed in $Ar:N_2$ encourages the conclusion that the orientational glass is a short-range-ordered variety of a ferroelastic and presumably ferroquadrupolar variety of the hcp structure, the long-range-ordered form of which has not been observed directly because it is screened by the $Pa3$ phase.

G. Application of hydrostatic pressure

For $0.75 \leq x \leq 0.8$, hydrostatic pressure increases the orthorhombic distortion and thereby the splitting of hcp (100) and (101) (Fig. 13), and reduces the inhomogeneous broadening. At $T=8$ K, $\Delta\gamma=0.8°$ at $p=1400$ bars and $\Delta\gamma=1.1°$ at $p=2200$ bars, compared to $\Delta\gamma=0.7°$ at zero pressure.

The sample with $x=0.82$ showed a peculiar behavior under pressure. When cooled down under a pressure of $p=1400$ bars, it entered from the hcp phase into the orientational glass state, suggesting that the threshold concentration x_c is changed to a value slightly larger than 0.82. If, on the other hand, this sample was cooled down into the $Pa3$ phase under zero pressure, the appli-

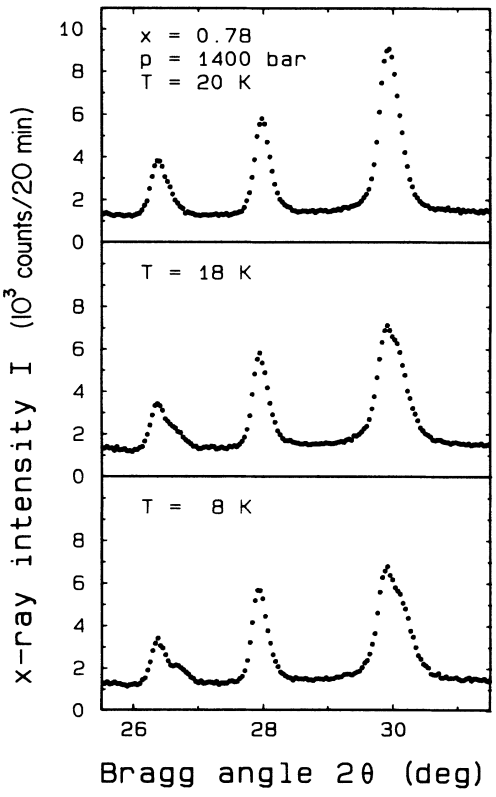

FIG. 13. Peak profiles of hcp (100), (002), and (101) reflections (from left to right) for a sample cooled under a pressure of 1400 bars. A splitting of (100) and (101) is due to the orthorhombic distortion.

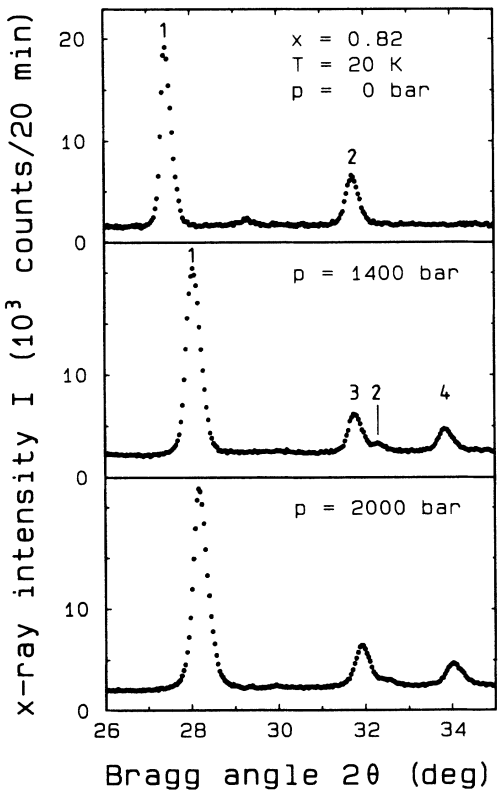

FIG. 14. X-ray-diffraction profiles of a sample cooled under its own vapor pressure and pressurized at $T=20$ K. For $p>1000$ bars tetragonal reflections occur, which grow approximately linearly with pressure at the expense of $Pa3$ reflections. 1, $Pa3$ (111) reflection and/or tetragonal (101); 2, $Pa3$ (200); 3, tetragonal (110); 4, tetragonal (002). At $p=1400$ bars the lattice parameters are $a=3.966\pm0.008$ Å and $c=5.266\pm0.01$ Å. For comparison, γ-N_2 at 4015 bars and 20.5 K (Ref. 38): $a=3.957$ Å and $c=5.109$ Å.

cation of pressure induced a transition into a new phase of tetragonal symmetry (Fig. 14). This phase is easily identified as the γ phase known as the high-pressure modification of pure N_2. Upon heating under pressure, the γ phase transforms back into the $Pa3$ phase at $T=30$ K, and finally into the hcp phase at $T=38$ K.

Summarizing, two families of structures have to be distinguished: the hexagonal phase with its glassy, slightly orthorhombically deformed offspring on one hand, and the cubic $Pa3$ phase with the high-pressure γ variety and the orientationally disordered fcc variety on the other. Transitions within the families are practically reversible; transitions between the families require a reconstruction of the center-of-mass lattice and are, therefore, to a very large extent, sluggish.

IV. SUMMARY AND CONCLUSIONS

The hcp-cubic transition has been identified as an athermal martensitic transformation with a large thermal hysteresis, coexistence regions, and an incomplete transformation in the vicinity of x_c. The similarity to the analogous transition in o-p-H_2 has been pointed out. The volume jump at the hcp-to-cubic transition and the slope of the transition line in the p,T phase diagram change sign at $x=0.85$. Referring to the Clausius-Clapeyron equation, the heats of transformation have been determined, which agree with the calorimetric results of Refs. 8 and 44 within experimental error. The hcp-to-cubic transition is accompanied by the orientational ordering of the N_2 molecules in the four-sublattice $Pa3$ pattern. Starting from the $Pa3$ state at low T, heating destroys the orientational order at T_{or}, whereas the fcc center-of-mass lattice is preserved up to $T_{ch} > T_{or}$. Thus for $T_{or} < T < T_{ch}$ an orientationally disordered fcc phase exists. The orientationally disordered fcc phase exists according to our results only for the mixed crystals, but not for pure N_2. It only appears when the cubic state can be superheated to sufficiently high T.

Stacking faults are abundant, both in the hcp and the cubic state. Our original presumption that the glasslike state might be understood as resulting from an incomplete transformation from a hcp to a fcc center-of-mass lattice, i.e., as a structure with a highly perturbed stacking sequence of the $(001)_{hex}$ planes, is not consistent with the present results. The diffraction profiles of the hcp lines in the orientational glass state instead suggest that random lattice strains develop with decreasing T, presumably due to the freezing of the N_2 orientations. This view is analogous to that of the mixed cyanides, and emphasizes the importance of the orientation-strain coupling.

The T dependence of the linewidth agrees with the T dependence of the "glass order parameter" q predicted by a random-bond–random-field Ising model. The best fits have been obtained for a combination of random bonds and weak random fields—q is essentially due to random bonds. Owing to the small random-field contribution, $q(T)$ has small nonzero values even at high T, and increases gradually with decreasing T.

A freezing temperature may be defined somewhat arbitrarily as temperature where the "glass order parameter," or correspondingly the linewidth, exceeds a certain fraction of its saturated low-temperature value, e.g., $\frac{1}{2}$ or $\frac{1}{3}$. The so-defined freezing temperatures are approximately concentration independent in the x range studied, $0.5 < x < x_c$.

In the orientational glass state a homogeneous strain component, corresponding to a slight orthorhombic distortion of the hexagonal unit cell, is superimposed on the random strains. This shear of the basal planes is presumably accompanied by slight changes of the in-plane orientational distribution of the N_2 molecules. The average inclination of the molecules with respect to the c axis does not change when the orthorhombic distortion occurs, as suggested by the smooth T dependence of the c/a ratio. The shape of the orientational distribution is slightly oblate, i.e., the average inclination angle with respect to the c axis is somewhat larger than the magic angle. With decreasing T there is a slight evolution towards the magic angle. Referring to the orthorhombic distortion, the existence of a ferroelastic and presumably ferroquadrupolar modification of hcp structure is suggested, the long-range-ordered form of which has not been observed directly because it is screened by the $Pa3$ phase. We suggest that the orientational glass can be seen as the short-range-ordered variety of this ferroelastic modification of hcp structure, and analogous ideas have been formulated for the mixed cyanides. The $Pa3$ phase, which is not a ferroelastic variety of hcp structure, does not seem to have any relevance to the orientational glass. This view is further supported by the fact that the high-pressure results suggest a division of the Ar:N_2 structural phases into two separate families not linked by group-subgroup relations. These two families are the hcp phase with its suggested ferroelastic modification and the orientational glass state on one hand, and the $Pa3$ phase with its tetragonal high-pressure product and with its disordered fcc variety on the other.

Harris and Meyer have argued[2] that the distinction between random bonds and random fields in the quadrupolar glasses is not as clear as in spin glasses. These authors have analyzed a random-bond Hamiltonian for a system of quadrupoles diluted on a rigid hcp lattice. The quadrupoles interact electrostatically. By use of replica mean-field theory, they show that the random-bond Hamiltonian can be separated into various terms, one of them having the form of a random-field term, another having the form of a Zeeman homogeneous field term. Thus the system studied experiences random and homogeneous quadrupole fields. It is appealing to regard the orthorhombic deformation of the present study as being due to the homogeneous quadrupole fields of Harris and Meyer. The gradual increase of our glass order parameter $q(T)$ is consistent with the presence of random fields. Thus we think that the analysis of Harris and Meyer is a good starting point for the understanding of Ar:N_2.

Recently, a certain universality of orientational glass formation has been cited, as suggested by the similarity of dielectric, thermodynamic, and NMR results of

$Ar:CO:N_2$ and of the cyanides. The present study supports this view by illuminating great analogies between these two systems concerning the structural aspects of orientational glass formation.

ACKNOWLEDGMENTS

This work has been supported by the Sonderforschungsbereich 262 of the Deutsche Forschungsgemeinschaft.

[1]F. Silvera, Rev. Mod. Phys. **52**, 393 (1980).

[2]A. Brooks Harris and H. Meyer, Can. J. Phys. **63**, 3 (1985).

[3]K. Knorr, Phys. Scr. **T19**, 531 (1987).

[4]W. Press, B. Janik, and H. Grimm, Z. Phys. B **49**, 9 (1982).

[5]D. Estève, N. S. Sullivan, and M. Devoret, J. Phys. (Paris) Lett. **43**, L793 (1982).

[6]N. S. Sullivan, C. M. Edwards, and J. R. Brookeman, Mol. Cryst. Liq. Cryst. **139**, 365 (1986)

[7]J. H. Walton, M.-C. Wu, and M. S. Conradi, Can. J. Chem. **66**, 680 (1988).

[8]L. G. Ward, A. M. Saleh, and D. G. Haase, Phys. Rev. B **27**, 1832 (1983).

[9]C. I. Nicholls, L. N. Yadon, D. G. Haase, and M. S. Conradi, Phys. Rev. Lett. **59**, 1317 (1987).

[10]L. N. Yadon, C. I. Nicholls, and D. G. Haase, Phys. Rev. B **40**, 5215 (1989).

[11]S. B. Liu and M. S. Conradi, Solid State Commun. **49**, 177 (1984).

[12]C. S. Barrett and L. Meyer, J. Chem. Phys. **42**, 107 (1965).

[13]For a review of the properties of N_2, see T. A. Scott, Phys. Rep. **27**, 89 (1976).

[14]W. E. Streib, T. H. Jordan, and W. N. Lipscomb, J. Chem. Phys. **37**, 2962 (1962).

[15]N. Krupskii, A. I. Prokhvatilov, and A. I. Erenburg, Fiz. Nizk. Temp. **1**, 359 (1975) [Sov. J. Low Temp. Phys. **1**, 178 (1975)].

[16]J. P. Sethna and K. S. Chow, Phase Transitions **5**, 317 (1985).

[17]K. H. Michel, Phys. Rev. Lett. **57**, 2188 (1986).

[18]K. H. Michel, Phys. Rev. B **35**, 1405 (1987); **35**, 1414 (1987).

[19]K. H. Michel, Z. Phys. B **68**, 259 (1987).

[20]C. Bostoen and K. H. Michel, Z. Phys. B **71**, 369 (1988).

[21]K. Binder and A. P. Young, Rev. Mod. Phys. **58**, 801 (1986).

[22]P. Goldbart and D. Sherrington, J. Phys. C **18**, 1923 (1985).

[23]M. Devoret and D. Estève, J. Phys. C **16**, 1827 (1983).

[24]H.-O. Carmesin and K. Binder, Europhys. Lett. **4**, 269 (1987); Z. Phys. B **68**, 375 (1987).

[25]H. Klee, H.-O. Carmesin, and K. Knorr, Phys. Rev. Lett. **61**, 1855 (1988).

[26]L. D. Yantsevich, A. I. Prokhvatilov, I. N. Krupskii, and A. S. Baryl'nik. Fiz. Nizk. Temp. **12**, 300 (1986) [Sov. J. Low Temp. Phys. **12**, 170 (1986)].

[27]J. L. Yarnell, R. L. Mills, and A. F. Schuch, Fiz. Nizk. Temp. **1**, 760 (1975) [Sov. J. Low Temp. Phys. **1**, 366 (1975)].

[28]S. Elschner, K. Knorr, and A. Loidl, Z. Phys. B **61**, 209 (1985).

[29]K. Knorr and A. Loidl, Phys. Rev. B **31**, 5387 (1985).

[30]K. Knorr and A. Loidl, Phys. Rev. Lett. **57**, 460 (1986).

[31]A. Loidl, T. Schräder, K. Knorr, R. Böhmer, M. Mertz, G. J. McIntyre, T. Vogt, H. Mutka, M. Müllner, H. Jex, and S. Haussühl, Z. Phys. B **75**, 81 (1989).

[32]A. Loidl, T. Schräder, R. Böhmer, K. Knorr, J. K. Kjems, and R. Born, Phys. Rev. B **34**, 1238 (1986).

[33]H. Miyagi and T. Nakamura, Prog. Theor. Phys. **37**, 641 (1967).

[34]H. M. James, Phys. Rev. **167**, 862 (1968).

[35]M. J. Mandell, J. Chem. Phys. **60**, 1432 (1974); **60**, 4880 (1974).

[36]K. A. Klenin and S. F. Pate, Physica **B+C 107B**, 185 (1981).

[37]M. A. Klenin, Phys. Rev. B **28**, 5199 (1983).

[38]A. F. Schuch and R. L. Mills, J. Chem. Phys. **52**, 6000 (1970).

[39]J. R. Brookeman and T. A. Scott, J. Low Temp. Phys. **12**, 491 (1973).

[40]P. Korpiun and E. Lüscher, in *Rare Gas Solids,* edited by M. L. Klein and J. A. Venables (Academic, London, 1976), p. 776.

[41]C. M. Wayman, in *Physical Metallurgy,* edited by R. W. Cahn and P. Haasen (North-Holland, Amsterdam, 1983), p. 1031.

[42]A. F. Schuch, R. L. Mills, and D. A. Depatie, Phys. Rev. **165**, 1032 (1968).

[43]D. Ramm, H. Meyer, and R. L. Mills, Phys. Rev. B **1**, 2763 (1970).

[44]E. L. Pace, J. H. Smith, and B. E. Jepson, J. Chem. Phys. **50**, 312 (1969).

[45]G. Pangilinan, G. Guelachvili, R. Sooryakumar, R. Narahari Rao, and R. H. Tipping, Phys. Rev. B **39**, 2522 (1989).

[46]D. G. Haase (private communication).

[47]A. Guinier, *X-Ray Diffraction in Crystals, Imperfect Crystals and Amorphous Bodies* (Freeman, San Francisco, 1963), Chaps. 6 and 7.

[48]B. E. Warren, *X-Ray Diffraction* (Addison-Wesley, New York, 1969), pp. 275–304. Our stacking-fault analysis was based on Eqs. 13.67 and 13.70 for the fcc lattice and on 13.86 for the hcp lattice.

[49]M. T. Sebastian and P. Krishna, *Progress in Crystal Growth and Characterization* (Pergamon, Oxford, 1987), Vol. 14, p. 103.

[50]R. Hosemann and S. N. Bagchi, *Direct Analysis of Diffraction by Matter* (North-Holland, Amsterdam, 1962), Chap. IX.

[51]T. R. Welberry, Rep. Prog. Phys. **48**, 1543 (1985).

[52]S. F. Edwards and P. W. Anderson, J. Phys. F **5**, 965 (1975); **6**, 1927 (1976).

[53]R. Pirc, B. Tadić, and R. Blinc, Phys. Rev. B **36**, 8607 (1987).

[54]S. Elschner, W. Wiotte, J. Petersson, and R. Blinc (unpublished); R. Blinc, Z. Naturforsch. **45A**, 313 (1990).

[55]R. Blinc, J. Dolinsek, R. Pirc, B. Tadić, B. Zalar, R. Kind, and O. Liechti, Phys. Rev. Lett. **63**, 2248 (1989).

[56]L. J. Lewis and M. L. Klein, Phys. Rev. Lett. **59**, 1837 (1987).

[57]K. Knorr, E. Civera-Garcia, and A. Loidl, Phys. Rev. B **35**, 4998 (1987).